Progress In Electromagnetics Research C, Vol. 79, 241–255, 2017

Development of Graphene Based Tapered Slot Antennas for Ultra-Wideband Applications

Reefat Inum*, Md. M. Rana, and Kamrun N. Shushama

Abstract—In this paper, three different types of graphene based tapered slot antennas are designed for ultra-wideband (UWB) applications. The taper profiles for three antenna types are linear, exponential, and constant width. A single layer graphene sheet of 35 μm thickness is used to model the radiating element and feeding structure of the designed antennas. To feed the antennas, microstrip to slotline transition technique is adopted. An approximate analytical theory based on conical transmission line model is considered to authenticate the design of graphene based tapered slot antennas. Better impedance matching over 2–20 GHz is obtained by designing a balun in the form of a radial stub. Return loss, bandwidth, radiation pattern, and directive gain are the considered antenna performance parameters. Time domain solver of CST MWS software is used to evaluate the performances of linearly tapered slot antenna (LTSA), exponentially tapered slot antenna (Vivaldi), and constant width slot antenna (CWSA). The results obtained from CST are compared with that from HFSS to further validate the design. Simulation results with extensive parametric study confirm that the novel 2-D material graphene can be considered as a promising one to model UWB tapered slot antennas. Furthermore, the effectiveness of designed graphene based tapered slot antennas is revealed by comparing their performances with other existing UWB antennas. Moreover, as a UWB application, Vivaldi antenna shows promising results in microwave brain tumor detection.

1. INTRODUCTION

According to Federal Communications Commission (FCC) of USA, ultra-wideband (UWB) frequency spectrum ranges from 3.1 GHz to 10.6 GHz [1, 2]. Recently, a surge of research interests has been created including the applications and investigations of UWB technology in the field of communications, radar and medical engineering [3]. The amount of RF bandwidth (> 500 MHz) that is achieved by UWB system mainly maximizes its performance. Nevertheless, successful operation of these systems relies on antennas that can efficiently radiate and receive UWB signals. So far, researchers have investigated different types of UWB antennas. Among them, tapered slot antenna (TSA) is a promising one for offering wide operational bandwidth, light weight, compact and planar size, and end-fire radiation characteristics [4–8].

However, most of the TSAs in the literature are built up of copper that are lagging in fulfilling the aforementioned performances perfectly [9–13]. In [4], a compact microstrip line-feed UWB tapered slot antenna on an FR4 substrate is presented. Besides using a tapered-shape slot etched out of the ground plane, a microstrip line-feed tuning stub is used to construct the antenna. Different tuning stubs namely rectangular, circular, elliptical, square and tapered shapes are investigated to tune the antenna performance. However, the best results obtained in terms of bandwidth and gain are 8.2 GHz and 5.4 dBi, respectively. A tapered slot antenna with rectangular slits is designed in [12]. The insertion

Received 26 July 2017, Accepted 17 November 2017, Scheduled 30 November 2017

* Corresponding author: Reefat Inum (romel.eee09@gmail.com).

The authors are with the Department of Electrical and Electronic Engineering, Rajshahi University of Engineering & Technology, Rajshahi-6204, Bangladesh.

of rectangular slits provides 8.45 GHz bandwidth and 7.55 dBi gain as confirmed by the measurement results. Therefore, consummate transmission and reception of UWB signals need an improvement in the TSA antennas concomitant with the advance of technology.

Graphene is a one atom thick planar sheet of carbon atoms tightly packed into a 2-D honeycomb crystal lattice [14], which is the substance with ability to replace the copper because of its characteristics of conductivity that is better than copper in scope of antenna. Since the discovery of this novel 2-D material, a variety of antenna types are studied based on graphene covering microwave to THz frequency range [15–19]. Although investigation of graphene based TSA still remains an unexplored area of research in the literature, some wideband and UWB antennas based on graphene have been designed and analyzed from different point of views recently. Specially, in the terahertz regime, the use of graphene in antenna design has attracted a wide research interest. For example, the benefit of reconfigurable graphene characteristics has been utilized in [15] to design an inset feed patch antenna for THz band application. The simulation results confirm that the antenna gain can be enhanced by incorporating a metamaterial layer and increasing the chemical potential of graphene. A Yagi antenna with graphene control has been developed in [16] for 1 THz applications. The reconfigurable characteristic of the antenna was obtained due to the tunable graphene conductivity. In microwave frequency range, flexible graphene based conductor (GBC) sheet is used to design a UWB antenna that shows an overall bandwidth of approximately 7.35 GHz and peak gain of 2.9 dB [17]. However, a comparative study reveals that the copper based antenna performs slightly better than GBC based one. Pattern reconfiguration by changing the bias voltage applied to the graphene is studied in [18] by designing a UWB dielectric coaxial hollow monopole antenna. Nevertheless, the effect of graphene as the conducting material on the performance of TSA with different tapering configurations is not reported so far.

In this paper, we design three different types of graphene based TSAs, namely LTSA, Vivaldi, and CWSA, for the first time. An approximate analytical theory [20] is considered to validate the design. The analytical model is based on conical transmission line approximation which concludes that antenna directive gain increases with frequency and radiation pattern differs completely in E and H-plane. To investigate the performance of the designed TSAs, a number of performance parameters such as return loss, VSWR, bandwidth, radiation pattern, and directive gain are calculated and analyzed. The performance of the TSAs is further optimized by designing a radial balun in conjunction with conducting an extensive parametric study. Analysis of radiation patterns and directive gain of the ultimate design coincide with the conclusions of the analytical model which validate the design. A performance comparison of the designed graphene based TSAs with some existing UWB antennas reported in the literature is presented to reveal the effectiveness of proposed design in addition to find out the taper profile for high performance graphene based TSA. Finally, graphene based Vivaldi antenna is suggested for a particular UWB application, i.e., microwave brain tumor detection and the results are presented.

2. MATERIALS AND METHODS

In this section, a brief description of frequency reconfigurable graphene surface conductivity for designing TSA in microwave frequency range is presented first. Next, a general analytical theory on TSA is given which is followed by a detail of antenna modeling procedure.

2.1. Graphene Material

The main advantage of using graphene in antenna design is the efficient dynamic tuning [15, 16]. Frequency dependent surface conductivity of graphene can be tuned by changing its chemical potential which is realized by adjusting a bias or gate voltage. This tunable property of graphene conductivity is utilized to tune the antenna resonance frequency, which in turn paves the way to design frequency reconfigurable antennas in microwave and THz regimes. Graphene based antennas could provide several other benefits including ease of integration, transparency and mechanical flexibility [21]. The frequency dependent 2-D surface conductivity of a single layer graphene sheet can be modeled using the well-known

Kubo formula as [22],

$$\sigma(\omega, \mu_c, \Gamma, T) \approx -j\frac{q_e^2 k_B T}{\pi\hbar^2(\omega - 2j\Gamma)} \times \left(\frac{\mu_c}{k_B T} + 2\ln\left(e^{-\frac{\mu_c}{k_B T}} + 1\right)\right) \quad (1)$$

where ω is the angular frequency, μ_c the chemical potential, $\Gamma = 1/2\tau$ the scattering rate where τ is the relaxation time, T the temperature, k_B the Boltzmann constant, and $\hbar^2$ the reduced Planck constant. However, to obtain reasonably accurate results for frequencies limited to microwave range, Equation (1) only considers intraband term. For varying chemical potential and a fixed relaxation time (τ), real and imaginary parts of the frequency dependent graphene surface conductivity is shown in Fig. 1. As evident from the figure, chemical potential can be treated as a key parameter to vary the conductivity which in turn tunes the resonance frequency.

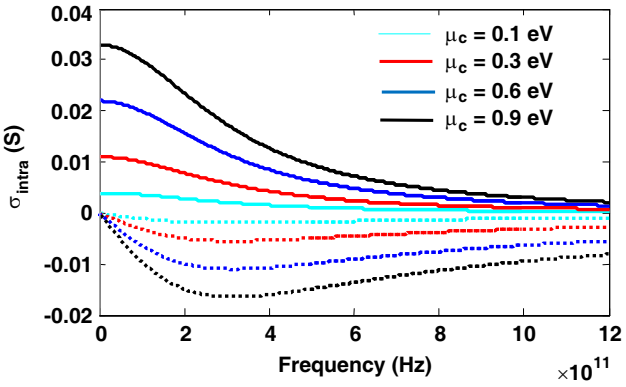

Figure 1. Real (solid) and imaginary (dashed) parts of the 2-D surface conductivity of graphene for varying μ_c with τ fixed at 0.1 ps.

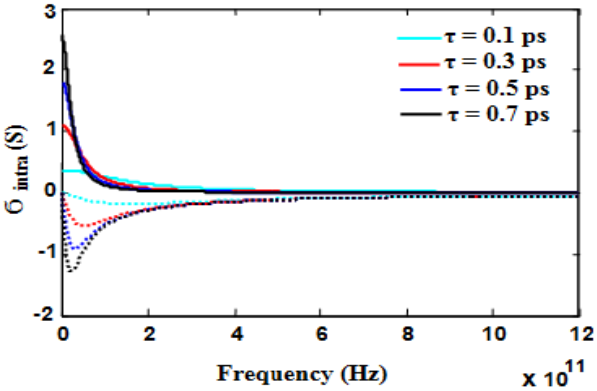

Figure 2. Real (solid) and imaginary (dashed) parts of the 2-D surface conductivity of graphene for varying τ with μ_c fixed at 1.5 eV.

Relaxation time (τ) is another factor to theoretically modify graphene's surface conductivity, which is related to scattering rate by the expression, $\Gamma = 1/2\tau$. As the main relaxation centers in graphene are charged impurities, any variation in relaxation time can alter electrical conductivity of graphene which is evident from Fig. 2. After conducting the parametric study of graphene conductivity in terms of chemical potential and relaxation time with temperature (T) fixed at 300 K, the optimum values of μ_c and τ are found to be 1.5 eV and 0.7 ps, which result in a graphene layer with minimum sheet resistance.

2.2. Analytical Theory for TSA Modeling

The choice of tapering profile of TSA affects the performance of antennas. Therefore, TSAs with different tapering profile correspond to different approximate analytical theory. For example, an approximate analytical theory is proposed in [23] to analyze the radiation patterns of LTSA. An approximate analytical form of Vivaldi on dielectric is proposed in [20], which is also claimed to be valid for all types of TSA.

In Fig. 3, the Vivaldi structure is approximated by using the opening angle and width gradually changing conical transmission line model. Consequently, the electromagnetic mode of each conical transmission line can be found and the basic mode is [20],

$$E_{\varphi'}^{(i)} = \frac{E_0}{\sin\left(\frac{\varphi_0^{(i)}}{2}\right)} \frac{1}{\sqrt{1 - \frac{\sin^2(\varphi')}{\sin^2\left(\frac{\varphi_0^{(i)}}{2}\right)}}} \times \sqrt{\frac{Z_c^{(i)}}{Z_c^{(i-1)}}} \frac{1}{r'} \times \left(Pe^{-k_i r'} + Qe^{k_i r'}\right) \quad (2)$$

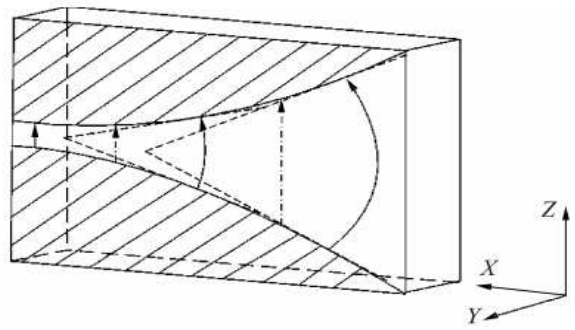

Figure 3. Field distribution of Vivaldi structure on dielectric [20].

where $E_{\varphi'}^{(i)}$ is the field distribution, φ' the observation angle, $\varphi_0^{(i)}$ the opening angle of the i-th sector, k_i the i-th wave number, and r' the distance from a field point to the source point. $Z_c^{(i-1)}$ and $Z_c^{(i)}$ are the characteristic impedance of $(i-1)$-th and i-th sectors, respectively, and P and Q are the incident and reflected waves, respectively. The radiation fields can be calculated from the azimuthal electric field distribution across the slot using Equation (2). This vector field can be decomposed into two components as,

$$E_{\varphi'} a_{\varphi'} = \cos(\varphi') E_{\varphi'} a_z + \sin(\varphi') E_{\varphi'} a_x \tag{3}$$

where, $a_{\varphi'}$, a_z, and a_x are the unit vectors. The radiated field can be given by Green's formalism as,

$$E^{(R)} = \iint_S E_{\varphi'} G \left[\cos(\varphi') a_z + \sin(\varphi') a_x\right] ds \tag{4}$$

where, S is the tapered slot aperture, and G is the dyadic Green's function [24], given as,

$$G = \begin{bmatrix} G_{\theta,z} & G_{\theta,x} \\ G_{\varphi,z} & G_{\varphi,x} \end{bmatrix} \tag{5}$$

where, $G_{\theta,z}$ and $G_{\theta,x}$ are the copolar radiated fields due to a longitudinal electric field source, while $G_{\varphi,z}$ and $G_{\varphi,x}$ yield the cross-polar radiated field due to a longitudinal and radial electric field source respectively. Through this analytical treatment, the radiation characteristics can be calculated which conclude that Vivaldi antenna's directive gain increases with the frequency and the patterns are different in E and H plane. The design of graphene based TSA in this paper is validated by fulfilling these two particular conditions.

2.3. Graphene Based TSA Design

Meanwhile, the antennas modeled in this work are illustrated in Fig. 4. The antennas are designed on the 0.8 mm thick Rogers RT5870 substrate with permittivity (ε_r) 2.33 and dissipation factor 0.0012. The size of the substrate is taken as $40 \times 45\,\text{mm}^2$. The projected antenna contains a microstrip feed line, microstrip to slot line transition, and the radiating structure. Radiation from the antennas takes place along the axis of tapered radiating structure. Theoretically unlimited bandwidth can be achieved by the continuous scaling and gradual curvature of the radiating structure, but practically slot line width, taper dimension, and transition from feed line are the factors to limit the theoretical bandwidth.

Figures 4(a), (b), and (c) depict the top view of Vivaldi antenna, LTSA, and CWSA, respectively. Length (L_1) and width (s) of the slotline, aperture length (L_2), edge offset (a), diameter (d) of the circular cavity, and length (L) and width (W) of substrate material are same for all the three TSAs. The dimension of the feeding structure including the radial balun is also same for three TSAs which are shown on the bottom part of antenna in Fig. 4(d). The taper profile of the Vivaldi antenna, i.e., exponential radiating curve is expressed as,

$$y(x) = Ae^{Bx} \tag{6}$$

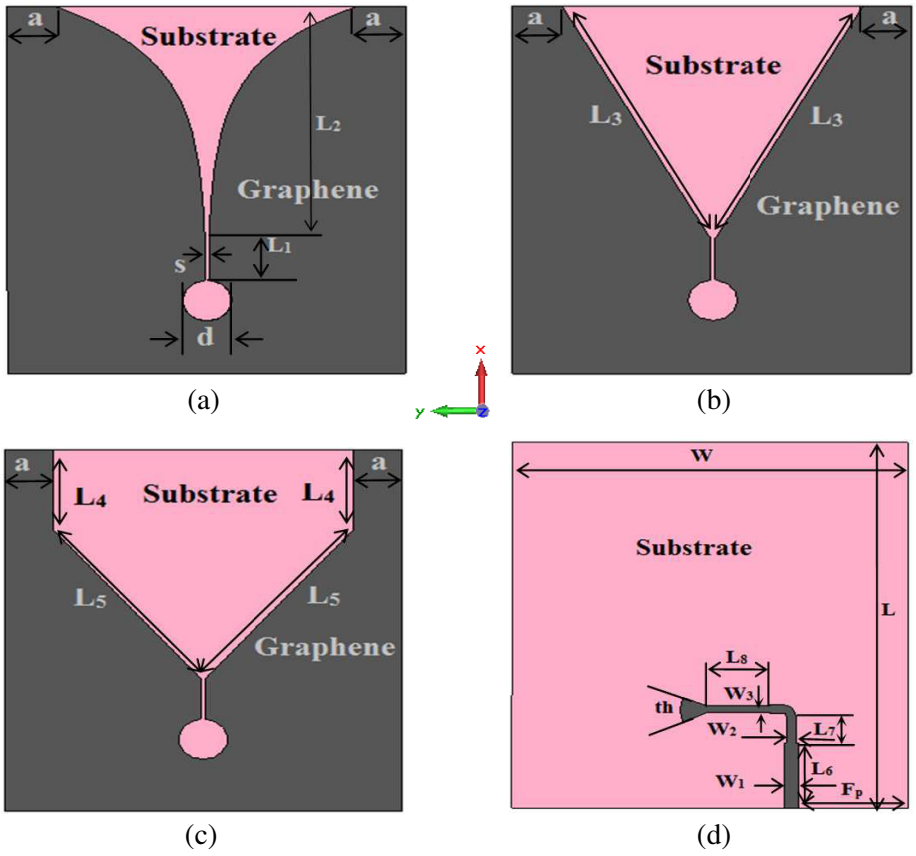

Figure 4. Geometry of the designed antennas, top view of (a) Vivaldi antenna, (b) LTSA, (c) CWSA, and (d) bottom view of either antenna.

where, constant A and opening rate B are given by,

$$A = \frac{s}{2} \tag{7}$$

$$B = \frac{1}{L_a} \ln\left(\frac{W_a}{s}\right) \tag{8}$$

where, L_a is the aperture length, W_a is the aperture width, and s is the slotline width. Aperture length is the effective length of tapering area which equals to L_2 in Fig. 4(a). Aperture width is taken equal to the substrate width. In Equation (6), y is the separation between the radiating curves at the origin and x is the length parameter. When x increases in the positive direction, the exponential radiating curves start flaring and the energy will have left the guiding structure. After a certain length (here, $x = L_2$), the exponential radiating curves will be truncated and the radiation in free space will take place. In the negative x-direction, the bonding between the EM wave and the conductors increases with increasing x which results in little radiation. In this direction, the curves are ended up in a circular cavity which acts as an open circuit to minimize the reflection of the stripline-slotline junction. Thus the theoretical infinite bandwidth of Vivaldi antenna is limited by the finite sized substrate, where the maximum positive and maximum negative x dimensions are controlled by the lowest and highest frequency respectively.

Edge offset (a) is considered as the key parameter to conduct parametric study in this work. Edge offset can be varied by varying either substrate width or opening rate. In this paper, to maintain a constant substrate width, a relation between edge offset and opening rate is developed so that the former can be varied with a variation in the later. Therefore, edge offset (a) is related to opening rate (B) by

the following expression,

$$B = \frac{1}{L_a} \ln\left(\frac{W_a}{(a+1)^{0.158} S}\right) \tag{9}$$

In the case of LTSA and CWSA, the tapering profile consists of straight line which can be constructed by simply joining two points in rectangular coordinate system. The straight radiation line can be expressed by well known straight line equation as,

$$y(x) = mx \tag{10}$$

where m is the slope of the straight line which gets steeper as the edge offset increases. However, in both the cases of LTSA and CWSA, the energy is strongly tied to the conductors at the starting of slotline in the negative x-direction and minute radiation takes place. When the length parameter x increases in the positive direction, the radiating line flares from each other and the EM energy starts leaving the guiding structure resulting in free space radiation. Meanwhile, the physical size of the antenna and the availability of fabrication capabilities limit the bandwidth of TSA. To arrive with respect to UWB band, the minimum frequency ($f_{\min}$) is taken as 2 GHz and the center frequency (f_c) is chosen as 10 GHz. With these frequency selections, the bound on the value of aperture width is calculated as follows [25],

$$W_{a\max} = \frac{\lambda_g}{2} \tag{11}$$

where λ_g is given by,

$$\lambda_g = \frac{c}{f_{\min}\sqrt{\varepsilon}} \tag{12}$$

where c is the speed of light (3×10^8 m/s), $f_{\min}$ the minimum frequency (2 GHz), and ε the dielectric constant (2.33) of the substrate. Putting these values in Equation (12), we have the value of λ_g which after substituting in Equation (11) gives the maximum aperture width ($W_{a\max}$) as 49 mm. The minimum value of the aperture width is calculated as,

$$W_{a\min} = \frac{c}{f_c\sqrt{\varepsilon}} \tag{13}$$

where f_c is the center frequency (10 GHz). After putting the values of all parameters in Equation (13), we have the value of minimum aperture width ($W_{a\min}$) as 19.65 mm. The TSAs designed in this paper maintain this bound of aperture width and thereby operate in the UWB band. Finally, Table 1 shows all the optimized dimension parameters to design the graphene based TSAs in this work.

Table 1. Optimized design parameters for graphene based TSAs.

Parameters	Dimension (mm)	Parameters	Dimension (mm)
W	40	L_5	23.84
L	45	L_6	8
L_1	5	L_7	3.2
L_2	28.5	L_8	1.3
s	0.4	W_1	1.5
d	5	W_2	1
a	5	W_3	0.75
L_3	32.23	th	45°
L_4	10	W_a	40

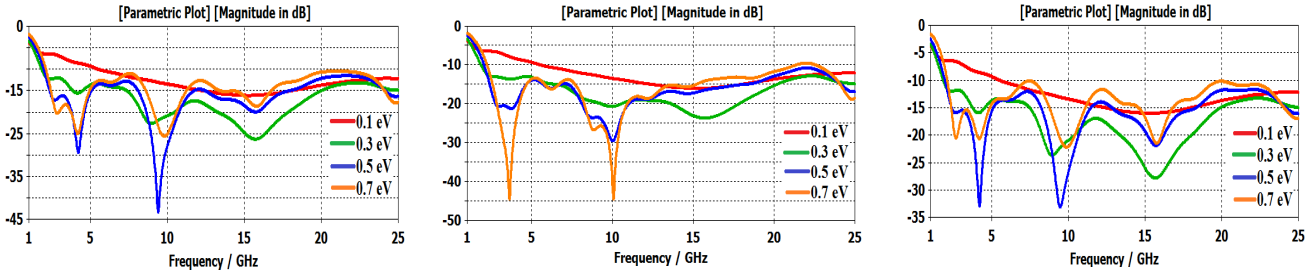

Figure 5. Reflection coefficient of (a) LTSA, (b) Vivaldi, (c) CWSA for varying chemical potential with $a = 0\,\text{mm}$.

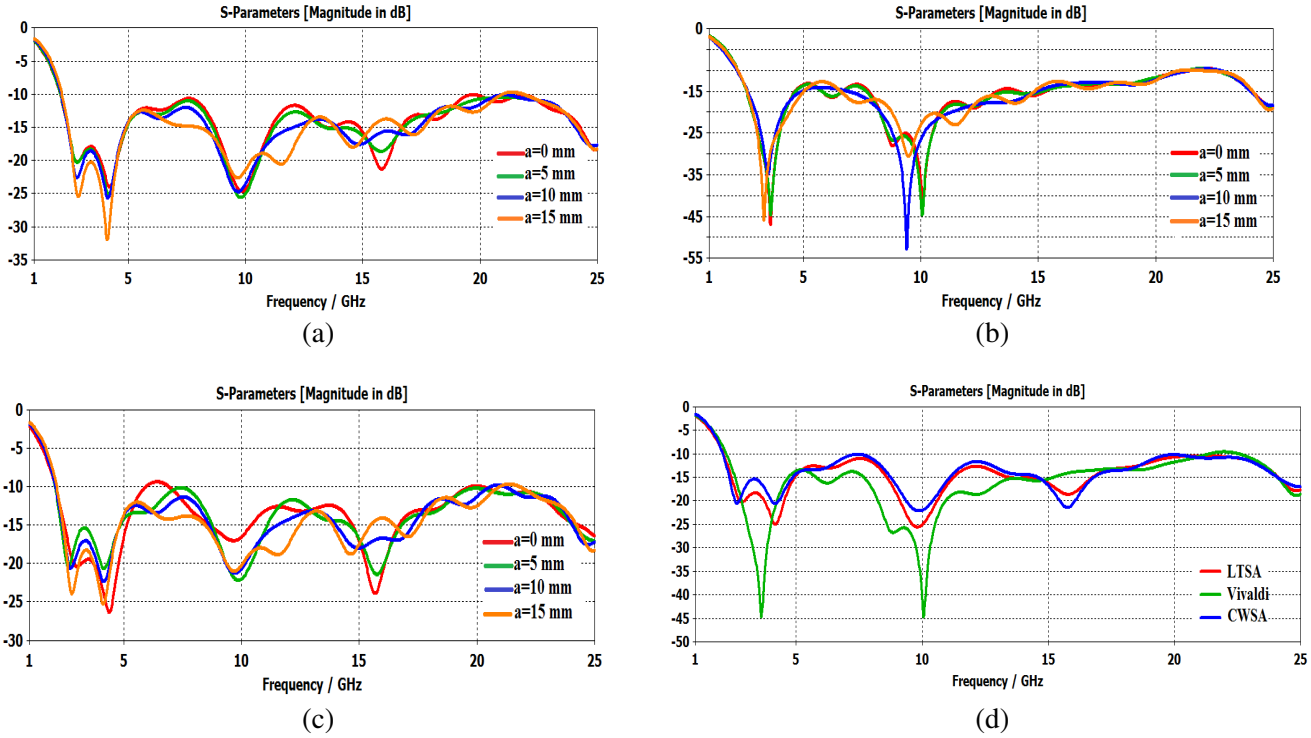

Figure 6. Reflection coefficient of (a) LTSA, (b) Vivaldi, and (c) CWSA for varying edge offset. (d) Comparison of reflection coefficient for LTSA, Vivaldi and CWSA with $a = 5\,\text{mm}$.

3. RESULTS AND DISCUSSIONS

To explore the usefulness of tunable surface conductivity of graphene in microwave antenna design, simulated reflection coefficients (S_{11}) of LTSA, Vivaldi and CWSA with the edge offset $a = 0\,\text{mm}$ are presented in Figs. 5(a), (b), and (c), respectively. Actually the scenarios in Fig. 5 are the inferences from Fig. 1 which justify the advantages of highly variable graphene conductivity to tune antenna resonant frequency. The relaxation time is considered as 0.1 ps in this case. It is observed from Fig. 5 that with zero edge offset, the reflection coefficient gets better linearly with increasing chemical potential for Vivaldi antenna while a discrepancy is found at 0.7 eV for LTSA and CWSA.

Next, the effect of changing edge offset (a) on each TSA is investigated which is observed in Fig. 6. To carry out this investigation, the optimum values of chemical potential (μ_c) and relaxation time (τ) are determined from Fig. 2. It is seen from Fig. 2 that the conductivity of graphene increases with τ for μ_c fixed at 1.5 eV, and for $\tau = 0.7\,\text{ps}$, resistance of graphene sheet is lowered sufficiently. Therefore,

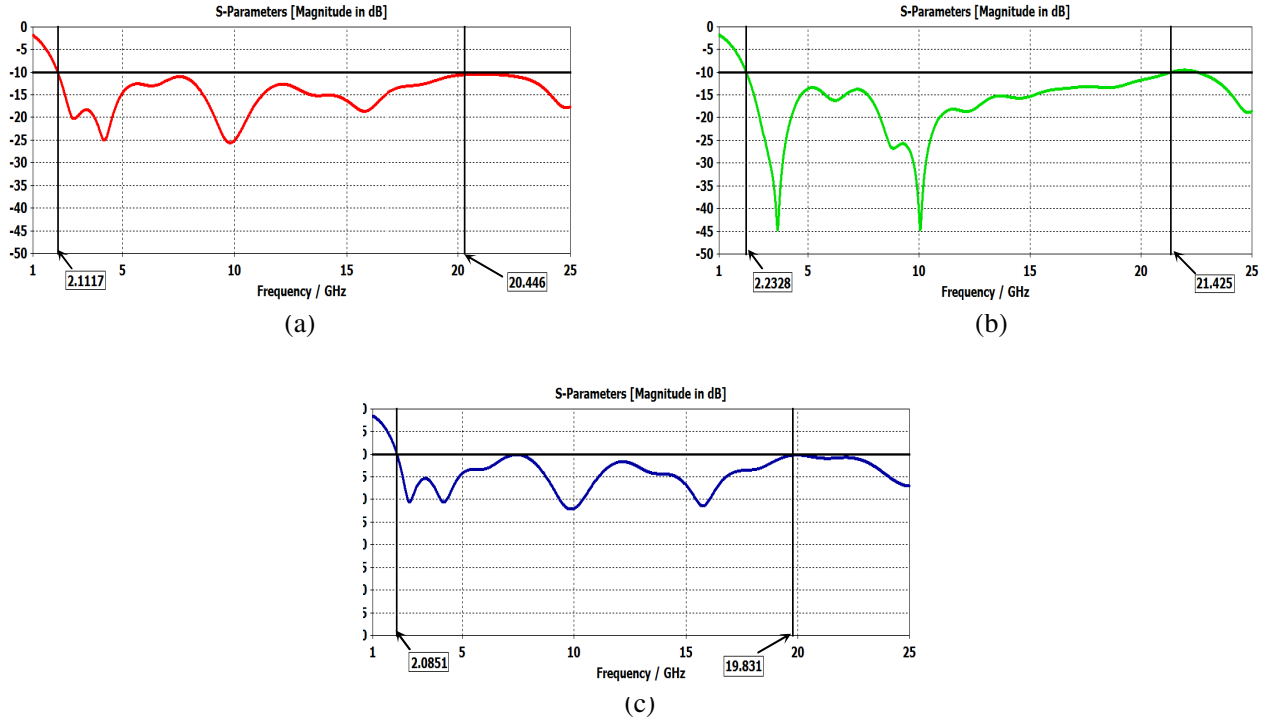

Figure 7. Reflection coefficients for $a = 5\,\text{mm}$ to evaluate the bandwidth of (a) LTSA, (b) Vivaldi and (c) CWSA.

optimal values of τ and μ_c are taken as 0.7 ps and 1.5 eV respectively, to model the monolayer graphene for the final TSA design. For $a = 15\,\text{mm}$, best reflection coefficient by LTSA is seen in Fig. 6(a). In this case, peak resonance occurs at low frequency region. Enhanced result in terms of reflection coefficient is obtained at $a = 10\,\text{mm}$ for Vivaldi antenna which is evident from Fig. 6(b). In this case, peak resonance occurs at relatively high frequency region compared to LTSA.

For CWSA, the best S_{11} is observed at $a = 15\,\text{mm}$ as shown in Fig. 6(c) where two resonance peaks are found at low frequency region. From Figs. 6(a), (b) and (c), it can be seen that all the three TSAs provide peak resonances at the centrer frequency 10 GHz for $a = 5\,\text{mm}$. Hence, a comparison of reflection coefficients between LTSA, Vivaldi and CWSA is made in Fig. 6(d) for the same edge offset ($a = 5\,\text{mm}$). It is observed from the figure that the Vivaldi antenna provides the best performance in terms of reflection coefficient than other two TSAs namely LTSA and CWSA.

In Fig. 7(a), the bandwidth performance in terms of return loss is evaluated for LTSA. The lower (f_L) and upper (f_H) frequencies at which the return loss curve crosses $-10\,\text{dB}$ are 2.1117 GHz and 20.446 GHz respectively. Therefore, return loss bandwidth of LTSA (RL BW_{LTSA}) is determined as follows,

$$\text{RL BW}_{\text{LTSA}} = f_H - f_L = 20.446 - 2.1117 = 18.334\,\text{GHz}$$

Similarly, Figs. 7(b) and (c) are used to evaluate the return loss bandwidth of Vivaldi (RL $\text{BW}_{\text{Vivaldi}}$) and CWSA (RL BW_{CWSA}) respectively. For the graphene based Vivaldi antenna, the evaluation of return loss bandwidth is as follows,

$$\text{RL BW}_{\text{Vivaldi}} = f_H - f_L = 21.425 - 2.2328 = 19.192\,\text{GHz}$$

In a similar manner, the return loss bandwidth of CWSA is evaluated by the following equation,

$$\text{RL BW}_{\text{CWSA}} = f_H - f_L = 19.831 - 2.0851 = 17.746\,\text{GHz}$$

For a center frequency (f_c) of 10 GHz for all the three TSAs, fractional bandwidths (FBW) provided by the LTSA, Vivaldi and CWSA are 183.3%, 191.9% and 177.5%, respectively. Therefore, from the

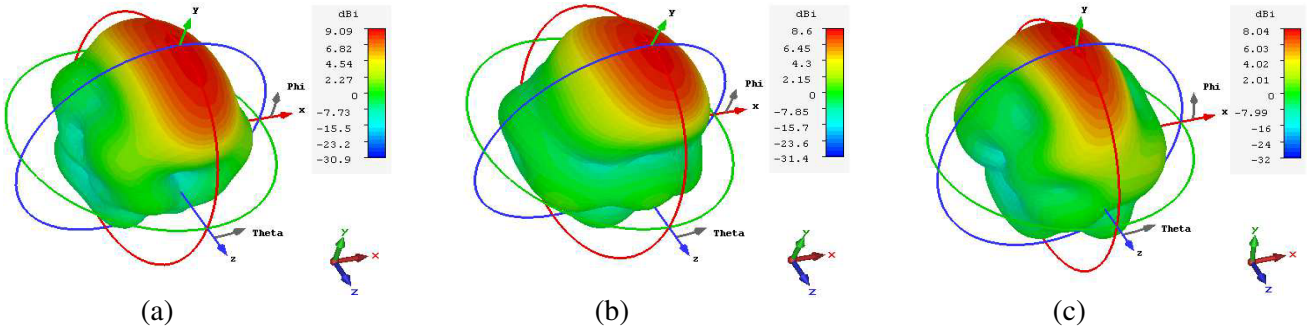

(a) (b) (c)

Figure 8. 3-D radiation patterns of (a) LTSA, (b) Vivaldi and (c) CWSA at the center frequency 10 GHz for $a = 5$ mm.

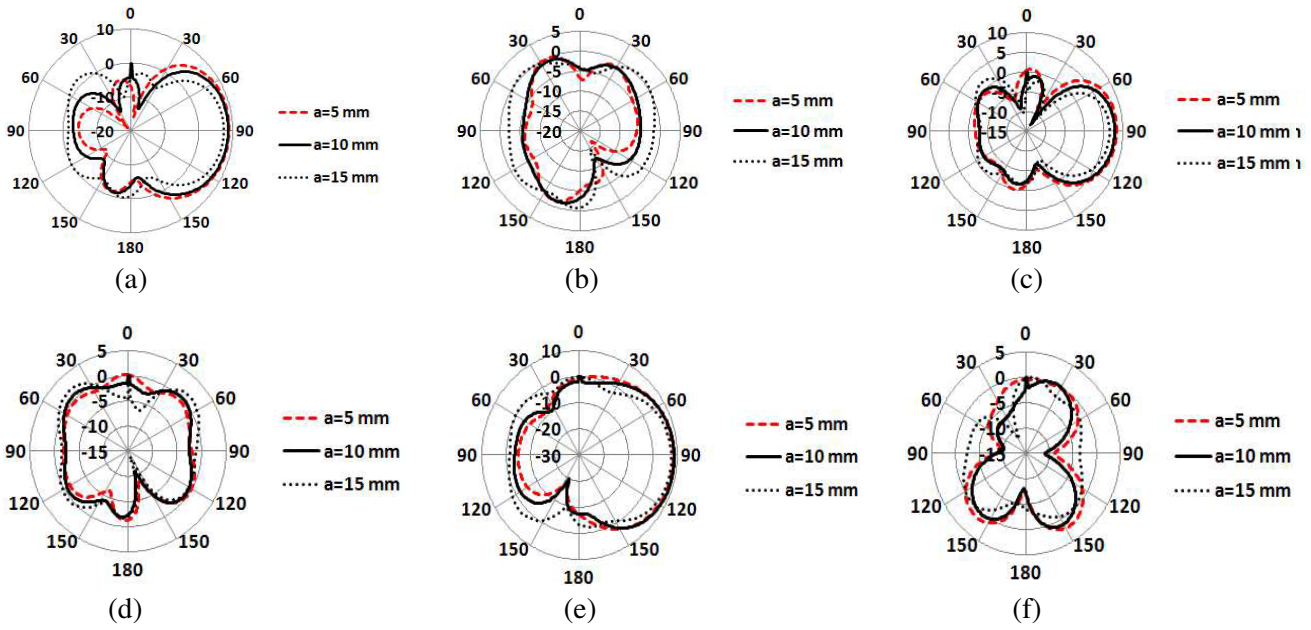

(a) (b) (c)

(d) (e) (f)

Figure 9. Radiation pattern of LTSA in (a) E-plane and (b) H-plane, Vivaldi in (c) E-plane and (d) H-plane, CWSA in (e) E-plane and (f) H-plane for varying edge offset.

above evaluation of bandwidth performance, it can be seen that the gaphene based Vivaldi antenna provides the best performance in terms of return loss bandwidth and FBW.

The 3-D radiation patterns of three TSAs, namely LTSA, Vivaldi, and CWSA at the center frequency 10 GHz with edge offset $a = 5$ mm, are shown in Fig. 8. At this particular frequency, peak resonances occur in the TSAs with edge offset $a = 5$ mm. Although end-fire radiation characteristics are observed from LTSA, Vivaldi, and CWSA in Figs. 8(a), (b), and (c) respectively, it is seen that the LTSA provides the highest directive gain in comparison to other two TSAs namely Vivaldi and CWSA.

Radiation characteristics of graphene based TSAs in E- and H-planes for varying edge offset (a) are described in Fig. 9. These patterns are recorded at 10 GHz so that differences in patterns can be analyzed at the same and relatively high frequency. Entirely different radiation patterns are observed in E- and H-planes for all the three antennas, which corresponds to one of the conclusions of the analytical model.

After confirming one of the conclusions of analytical TSA model, i.e., different patterns in E- and H-planes, change of directive gain with frequency is studied to ascertain another condition. Fig. 10 is plotted to investigate how the directive gain reacts to frequency change. The effect of edge offset on directive gain is also studied in the same figure. For all the TSAs, itis observed from Figs. 10(a), (b),

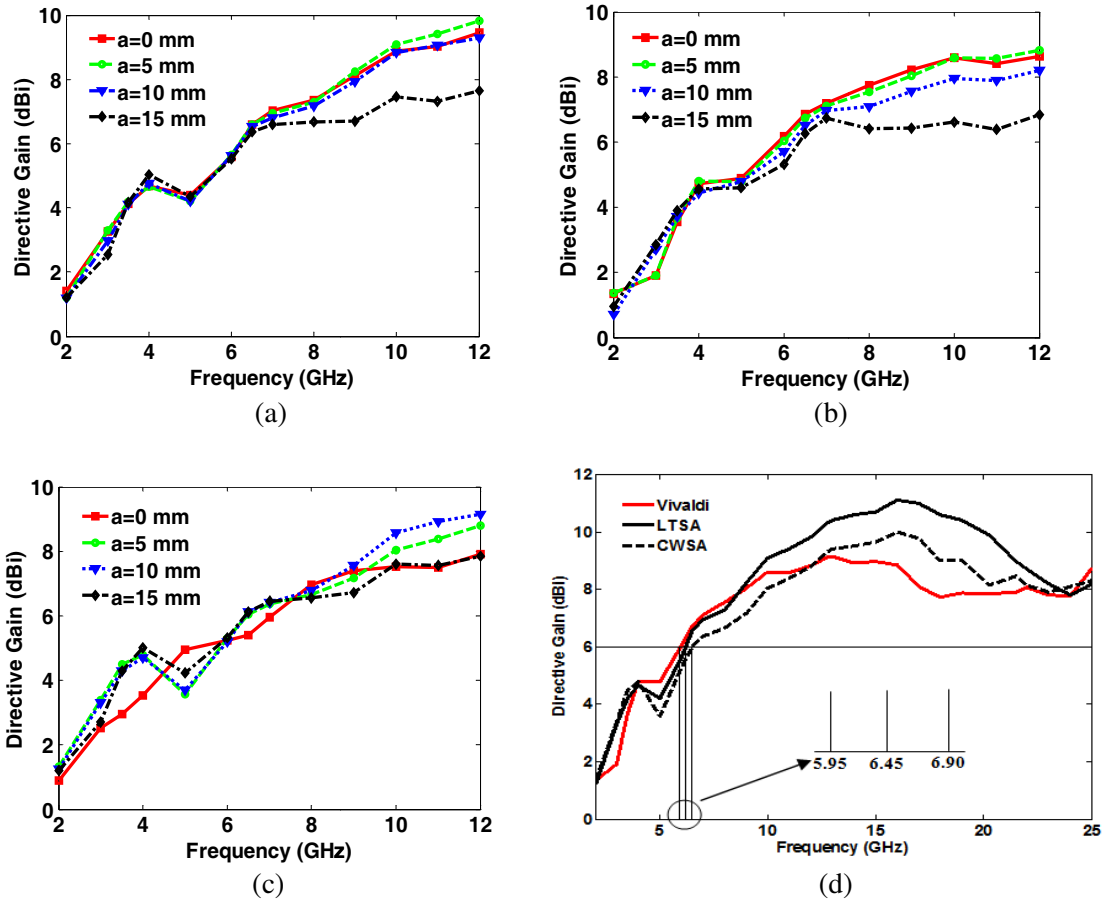

Figure 10. Directive gain (dBi) versus frequency plot for (a) LTSA, (b) Vivaldi, and (c) CWSA with varying edge offset, (d) comparison of directive gain for LTSA, Vivaldi, and CWSA with $a = 5\,\text{mm}$.

and (c) that the directive gain increases with an increase in frequency, which agrees with the conclusion of analytical model.

While investigating the effect of edge offset on the directive gain, it is found from Fig. 10(a) that an increase in edge offset degrades the directive gain for LTSA. In this case, the best result is obtained for $a = 5\,\text{mm}$. In general, it can be concluded that the steeper the slope of graphene based LTSA is, the lesser the directive gain is achieved. Fig. 10(b) reveals that the same conclusion can be drawn for Vivaldi antenna as LTSA. In this case also, better increase in directive gain with frequency is found for $a = 5\,\text{mm}$, and as a whole, directive gain degrades with an increase in edge offset. For CWSA, it is seen from Fig. 10(c) that $a = 10\,\text{mm}$ gives the best result in terms of directive gain versus frequency. Nevertheless, CWSA opposes other two TSAs in that its directive gain increases with an increase in edge offset from 0 to 10 mm. For $a = 15\,\text{mm}$, directive gain decreases which can be treated as an exception as for $a = 5\,\text{mm}$ in the case of LTSA and Vivaldi antennas. Finally, a comparison of directive gain for three graphene based TSAs with edge offset fixed at 5 mm is illustrated in Fig. 10(d), where the frequency range is extended to 25 GHz so that gain bandwidth can be determined properly. It can be concluded from this figure that graphene based LTSA for $a = 5\,\text{mm}$ provides the best directive gain in relatively high frequency region. This is because there is no discontinuity in the tapering profile of LTSA, and hence surface current can travel along the linear tapering with relative ease as compared to Vivaldi antenna and CWSA. However, in the low frequency region, conventional exponential tapering (Vivaldi) performs the best in terms of directive gain, which is extremely advantageous in UWB application like microwave imaging for brain tumor detection.

Gain bandwidth (GBW) of the designed TSAs can be determined from Fig. 10(d), where the

highest frequency (f_H) is same (25 GHz) for all the three TSAs. The lowest frequencies (f_L) assuming 6 dBi as the reference gain for LTSA, Vivaldi and CWSA are 6.45 GHz, 5.95 GHz and 6.90 GHz, respectively. Therefore, the following calculations are carried out to determine the gain bandwidth of LTSA (GBW_{LTSA}), Vivaldi ($\text{GBW}_{\text{Vivaldi}}$) and CWSA ($\text{GBW}_{\text{CWSA}}$):

$$GBW_{\text{LTSA}} = f_H - f_L = 25 - 6.45 = 18.55\,\text{GHz}$$
$$GBW_{\text{Vivaldi}} = f_H - f_L = 25 - 5.95 = 19.05\,\text{GHz}$$
$$GBW_{\text{CWSA}} = f_H - f_L = 25 - 6.90 = 18.10\,\text{GHz}$$

Thus, graphene based Vivaldi antenna outperforms other TSAs in terms of gain bandwidth also. It is also observed that the gain bandwidth is different from return loss bandwidth because the highest frequency is same for all the three TSAs in the case of gain bandwidth.

Table 2. Performance comparison of the designed graphene based TSAs with other UWB antennas.

Performance parameters	Designed TSAs			Conventional antennas			Graphene based antennas	
	LTSA	Vivaldi	CWSA	[4]	[11]	[12]	[17]	[18]
Return loss (dB)	−32.03	−52.85	−25.28	−32.50	−40.00	−64.40	−25.23	−39.92
VSWR	1.05	1.00	1.12	1.06	NR	1.04	NR	NR
Peak gain (dBi)	9.09	8.60	8.58	5.4	15	7.55	4.83	NR
Bandwidth (GHz)	18.334	19.192	17.746	8.2	19	8.45	7.35	4.0

NR — Not reported

The efficacy of modeled graphene based TSAs is analyzed by comparing their performances with other existing UWB antennas as shown in Table 2. It is observed from this table that the graphene based TSAs designed in this work provide enhanced outcomes as compared to other UWB antennas reported in the literature except [11]. A novel technique using composite aperture structure was proposed in [11] to achieve linear phase center in the end-fire taper slot Vivaldi antenna. The simulation and experimental results show that the proposed model is able to operate in a wide bandwidth of 3–22 GHz with a peak gain of 15 dBi. Thus, careful engineering in the structure of copper based TSA can provide higher gain than the graphene based one. However, while comparing among different taper profiles, it can be said that the exponential tapering is the best for improved impedance matching. Morever, in terms of directive gain, linear and exponential tapering perform better in the relatively high and low frequency regions respectively. Nevertheless, the simulation results obtained by CWSA are also appreciable as compared to other conventional and graphene based UWB antennas.

Finally, the validation of the designed TSAs is done by simulating the same antennas with another software HFSS and comparing the results. Figs. 11 and 12 provide the simulation results in terms of reflection coefficient and E-plane radiation pattern respectively, obtained from CST and HFSS software. From Fig. 11, a close agreement of S_{11} obtained from CST and HFSS is observed, which indicates a validation of our design. Although slight deviation in side lobe level is found, a better agreement in case of peak gain and main lobe direction is observed for E-plane radiation patterns in Fig. 12. These patterns are plotted at the center frequency 10 GHz with an edge offset of 5 mm.

4. APPLICATION OF THE TSA IN UWB MICROWAVE BRAIN IMAGING

From the performance comparison available in Table 2, graphene based Vivaldi antenna is suggested for the human brain tumor detection using UWB microwave brain imaging technique. Such an application usually requires a larger bandwidth to ensure minimum distortion and dispersion on the transmitted or

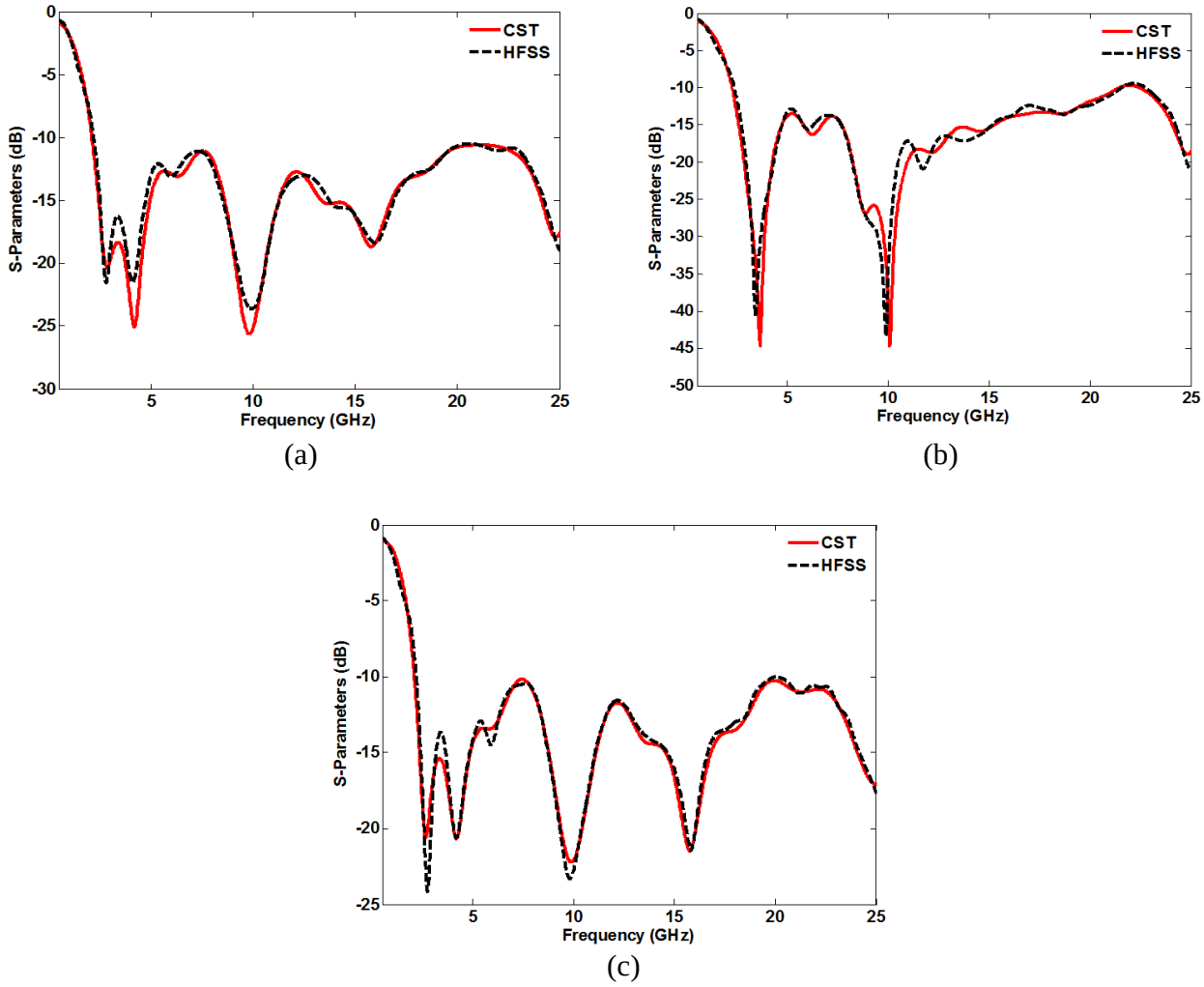

Figure 11. Reflection coefficients of (a) LTSA, (b) Vivaldi and (c) CWSA by CST and HFSS with edge offset $a = 5\,\text{mm}$.

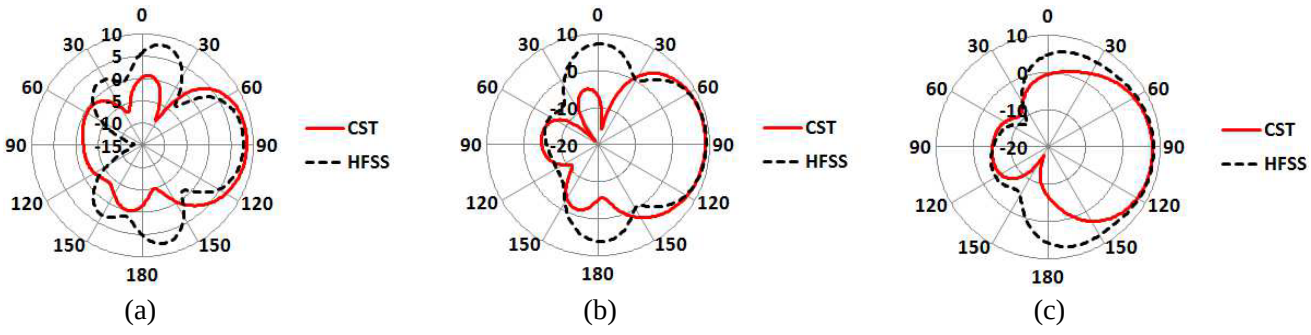

Figure 12. *E*-plane radiation patterns of (a) Vivaldi, (b) LTSA and (c) CWSA obtained from CST and HFSS at 10 GHz with edge offset of 5 mm.

received signals. On this application, an antenna with directive pattern, improved return loss, VSWR and gain is highly desirable. The suggested antenna can fulfill these requirements and thus successfully be utilized in brain tumor detection application. However, to verify the application of the suggested antenna in brain tumor detection, a four-layered human head model with tumor inside it is used in

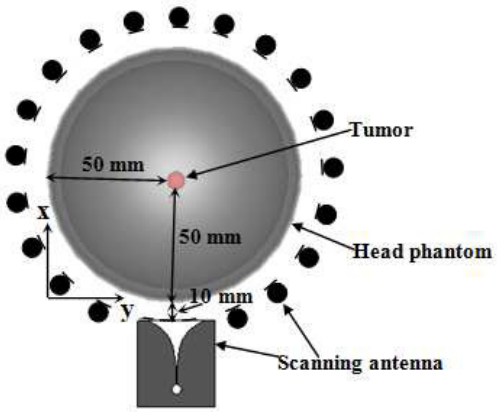

Figure 13. Geometrical setup for cylindrical scanning.

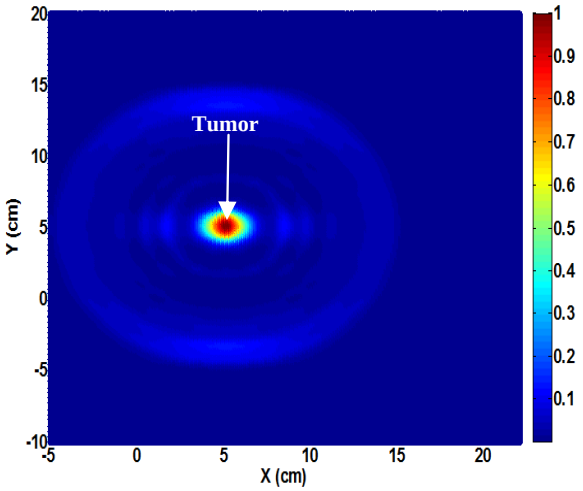

Figure 14. Reconstructed microwave image of tumor by scanning the head phantom with graphene based Vivaldi antenna.

the simulation [26]. Among the four head tissue layers, the inner layer is the white matter with a radious of 93 mm and the other layers are bone, fat and skin with thickness of 5 mm, 1 mm and 1 mm respectively. The dielectric properties of these tissues are obtained from the material library of CST MWS software. The dimension and dielectric properties of tumor are taken from [26]. Mono-static radar based microwave imaging technique is utilised in this case where a single antenna scans the head phantom. Graphene based Vivaldi antenna with edge offset of 5 mm is chosen as the scanning antenna among three TSAs, because it provides better directive gain in relatively low frequency region, which is extremely useful for penetrating the head tissue layers. Cylindrical scan mode is adopted where the scanning is done by rotating the antenna around the head phantom, as displayed in Fig. 13. It uses a fixed number of rotation steps, for which the cylindrical rotation index, referred to as i, takes integer values ranging from 1 to 360 degrees. Here 36 antenna positions are used to illuminate the whole phantom region, therefore the angular step between two adjacent antenna positions is 10 degree. The distance between the scanning antenna and the phantom surface is taken as 10 mm. At each antenna stop position, the phantom is simulated and the frequency domain scattering signal is collected. This received signal includes reflections from different head tissue layers, clutters and tumor response. To extract the tumor response from this received signal, a reference signal is obtained by simulating a head phantom without tumor inside it. The received and reference signals are transformed from frequency to time domain by Inverse Fast Fourier Transform (IFFT). Then the time domain tumor response is obtained by subtracting the reference signal from the received signal. This tumor response still contains some clutter due to reflection from antennas. In order to reduce the reflections due to antenna, the tumor response is first averaged and then subtracting the averaged signal from the tumor response for each antenna position. After that, synthetic focusing is performed and finally the intensity values are calculated and plotted to generate a continuous color image as shown in Fig. 14. High intensity of colors indicates positions of significant scatterers (tumor) inside the head. It is clear from Fig. 14 that the designed graphene based Vivaldi antenna has the potential to detect tumor inside human head using UWB microwave imaging technique.

5. CONCLUSION

The design of graphene based tapered slot antenna (TSA) for ultra-wideband applications is reported. The effect of a single layer graphene sheet of 35 µm thickness as the radiating element and feeding structure on the performance of linear tapered slot antenna (LTSA), exponential tapered slot antenna (Vivaldi), and constant width slot antenna (CWSA) is investigated. An approximate analytical theory

is considered to assess the design of TSAs. Simulation results show that the designed TSAs possess the characteristics as concluded in the analytical theory which confirms our design. While conducting parametric study, the optimum value of the edge offset (a) is found to be 5 mm, for which all the three TSAs show peak resonances at the center frequency 10 GHz. In terms of directive gain, LTSA performs the best in relatively high frequency region and Vivaldi antenna provides enhanced result in low frequency region. The tendency of graphene based Vivaldi antenna to provide higher gain in relatively low frequency region is absolutely beneficial in UWB radar based microwave imaging, in order to obtain sufficient penetration depth of the transmitted signal inside the dielectric tissue layers and fairly good resolution of the reconstructed image. Therefore, graphene based Vivaldi antenna is selected for a particular UWB application, i.e., microwave brain imaging for brain tumor detection, due to its improved performances in comparison to other two TSAs. The reconstructed tumor image indicates that the suggested antenna has the potential to be reliably utilised in such UWB application, and the study conducted in this paper is expected to be helpful for the future research on graphene based TSA modeling.

REFERENCES

1. The Federal Communications Commission, "Revision of Part 15 of the Commision's rules regarding ultra wideband transmission systems," First report and order, FCC 02-48, Washington, DC, USA, Apr. 2002.
2. The Federal Communications Commission, "Revision of Part 15 of the Commision's rules regarding ultra wideband transmission systems," First report and order, FCC 03-33, Washington, DC, USA, Sep. 2007.
3. Rahayu, Y., T. A. Rahman, R. Ngah, and P. S. Hall, "Ultra wideband technology and its applications," *5th IFIP International Conference on Wireless and Optical Communications Networks*, May 2008.
4. Azim, R., M. T. Islam, and N. Misran, "Compact tapered-shape slot antenna for UWB applications," *IEEE Antennas and Wireless Propagation Letters*, Vol. 10, 1190–1193, Oct. 2011.
5. Yao, Y., M. Liu, W. Chen, and Z. Feng, "Analysis and design of wideband widescan planar tapered slot antenna array," *IET Microw. Antennas Propag.*, Vol. 4, No. 10, 1632–1638, 2010.
6. Jolani, F., G. Dadashzadeh, M. Naser-Moghadasi, and A. Dadgarpour, "Design and optimization of compact balanced antipodal vivaldi antenna," *Progress In Electromagnetics Research C*, Vol. 9, 183–192, 2009.
7. Ramesh, S. and T. Rama Rao, "Dielectric loaded exponentially tapered slot antenna for wireless communications at 60 GHz," *Progress In Electromagnetics Research C*, Vol. 38, 43–54, 2013.
8. Kwame, O. G., G. Wen, Y. Huang, A. E. Ampoma, and W. Hu, "Broadband circularly polarized cross shaped slot antenna with an improved feedline," *Progress In Electromagnetics Research C*, Vol. 74, 141–149, 2017.
9. Lee, D.-H., H.-Y. Yang, and Y.-K. Cho, "Design and analysis of tapered slot antenna with 3.5/5.5 GHz band-Notched characteristics," *Progress In Electromagnetic Research B*, Vol. 56, 347–363, 2013.
10. Cicchetti, R., E. Miozzi, and O. Testa, "Wideband and UWB antennas for wireless applications: A comprehensive review," *International Journal of Antennas and Propagation*, Vol. 2017, 1–45, Hindawi, Feb. 2017.
11. Arezoomand, A. S., R. A. Sadeghzadeh, and M. N. Moghadasi, "Novel techniques in tapered slot antenna for linearity phase center and gain enhancement," *IEEE Antennas and Wireless Propagation Letters*, Vol. 16, 270–273, 2017.
12. Kim, S. W. and D. Y. Choi, "Implementation of rectangular slit-inserted ultra-wideband tapered slot antenna," *Springerplus*, Vol. 5, No. 1, 1–11, Aug. 2016.
13. Low, X. N., Z. N. Chen, and T. S. P. See, "A UWB dipole antenna with enhanced impedance and gain performance," *IEEE Trans. Antennas Propag.*, Vol. 57, No. 10, 2959–2966, 2009.

14. Geim, A. K. and K. S. Novoselov, "The rise of graphene," *Nature Materials*, Vol. 6, No. 3, 183–191, Mar. 2007.
15. Seyedsharbaty, M. M. and R. A. Sadeghzadeh, "Antenna gain enhancement by using metamaterial radome at THz band with reconfigurable characteristics based on graphene load," *Opt. Quant. Electron.*, Vol. 46, No. 221, 2017.
16. Zarrabi, F. B., et al., "Wide band Yagi antenna for terahertz application with graphene control," *Optik — Int. J. Light Electron Optics*, 2017, doi: http://dx.doi.org/doi:10.1016/j.ijleo.2017.05.009.
17. Asif, S. M., A. Iftikhar, B. D. Braaten, and M. S. Khan, "Design of an ultra-wideband antenna using flexible graphene-based conductor sheets," *IEEE International Symposium on Antennas and Propagation*, 1863–1864, 2016.
18. Jiang, Y., R. Yuan, X. Gao, J. Wang, S. Li, and Y. Lin, "An ultra-wideband pattern reconfigurable antenna based on graphene coating," *Chin. Phys. B*, Vol. 25, No. 11, 1–7, 2016.
19. Kopyt, P., et al., "Graphene-based dipole antenna for a UHF RFID tag," *IEEE Trans. Antennas Propag.*, 2016, doi: 10.1109/TAP.2016.2565696.
20. Yao, Y., W. Chen, B. Huang, Z. Feng, and Z. Zhang, "Analysis and design of tapered slot antenna for ultra-wideband applications," *Tsinghua Science and Technology*, Vol. 14, No. 1, 1–6, Feb. 2009.
21. Inum, R. M., M. Rana, and K. N. Shushama, "Performance analysis of graphene based nano dipole antenna on stacked substrate," *Int. Conf. Electrical, Computer and Telecommunication Engineering*, Rajshahi, Mar. 2017, doi: 10.1109/ICECTE.2016.7879574.
22. Hanson, G. W., "Dyadic Greens functions and guided surface waves for a surface conductivity model of graphene," *J. Appl. Phys.*, Vol. 103, No. 6, Mar. 2008.
23. Stockbroeckx, B. and A. V. Vorst, "Electromagnetic modes in conical transmission lines with application to the linearly tapered slot antenna," *IEEE Trans. Antennas Propag.*, Vol. 48, No. 3, 447–455, Mar. 2000.
24. Tai, C.-T., *Dyadic Green Functions in Electromagnetic Theory*, 2nd Edition, IEEE Press, 1994.
25. Shin, J. and D. H. Schaubert, "A parameter study of stripline-fed vivaldi notch-antenna arrays," *IEEE Trans. Antennas Propag.*, Vol. 47, No. 5, 879–886, May 1999.
26. Zhang, H., et al., "A smart antenna array for brain cancer detection," *Loughborough Antennas & Propagation Conference*, 1–4, Loughborough, UK, Nov. 2011.